Combined Proteomic and Cytological Analysis of Ca^{2+}-Calmodulin Regulation in *Picea meyeri* Pollen Tube Growth[1][C][W]

Tong Chen, Xiaoqin Wu, Yanmei Chen, Xiaojuan Li, Mei Huang, Maozhong Zheng, František Baluška, Jozef Šamaj, and Jinxing Lin*

Key Laboratory of Photosynthesis and Molecular Environmental Physiology, Institute of Botany, Chinese Academy of Sciences, Beijing 100093, China (T.C., X.W., Y.C., X.L., M.H., M.Z., J.L.); Systematic and Evolutionary Botany, South China Botanical Garden, Chinese Academy of Sciences, Guangzhou 510650, China (X.W.); Graduate School of Chinese Academy of Sciences, Beijing 100039, China (M.Z.); Institute of Cellular and Molecular Botany, University of Bonn, D–53115 Bonn, Germany (F.B., J.Š.); Institute of Plant Genetics and Biotechnology, Slovak Academy of Sciences, SK–95007 Nitra, Slovak Republic (J.Š.); and Faculty of Natural Sciences, Palacký University Olomouc, 771 47 Olomouc, Czech Republic (J.Š.)

Ca^{2+}-calmodulin (Ca^{2+}-CaM) is a critical molecule that mediates cellular functions by interacting with various metabolic and signaling pathways. However, the protein expression patterns and accompanying serial cytological responses in Ca^{2+}-CaM signaling deficiency remain enigmatic. Here, we provide a global analysis of the cytological responses and significant alterations in protein expression profiles after trifluoperazine treatment in *Picea meyeri*, which abrogates Ca^{2+}-CaM signaling. Ninety-three differentially displayed proteins were identified by comparative proteomics at different development stages and were assigned to different functional categories closely related to tip growth machinery. The inhibition of Ca^{2+}-CaM signaling rapidly induced an increase in extracellular Ca^{2+} influx, resulting in dramatically increased cytosolic Ca^{2+} concentrations and ultrastructural abnormalities in organelles as the primary responses. Secondary and tertiary alterations included actin filament depolymerization, disrupted patterns of endocytosis and exocytosis, and cell wall remodeling, ultimately resulting in perturbed pollen tube extension. In parallel with these cytological events, time-course experiments revealed that most differentially expressed proteins showed time-dependent quantitative changes (i.e. some signaling proteins and proteins involved in organelle functions and energy production changed first, followed by alterations in proteins related to cytoskeletal organization, secretory pathways, and polysaccharide synthesis). Taken together, Ca^{2+}-CaM dysfunction induced serial cytological responses and temporal changes in protein expression profiles, indicating the pivotal role of Ca^{2+}-CaM in the regulation of tip growth machinery.

The pollen tube delivers male gametes to the egg in flowering plants and is thus essential for sexual reproduction. Pollen tubes represent an ideal model system with which to investigate polarized growth in plant cells. They exhibit a tip-focused cytosolic Ca^{2+} concentration ([Ca^{2+}]$_c$) cellular gradient that is established mainly by extracellular Ca^{2+} influx whereby both intracellular [Ca^{2+}]$_c$ and extracellular Ca^{2+} influx exhibit oscillations that are accompanied by oscillations in growth rate (Cheung and Wu, 2001, 2008; Gilroy and Trewavas, 2001; Feijo et al., 2004). The Ca^{2+} signatures must be sensed, interpreted, and transduced to downstream components by specific molecular decoders such as calmodulin (CaM), which is a protein that possesses a helix-loop-helix (EF-hand) motif.

CaM is a highly conserved regulatory protein that is ubiquitous in eukaryotic cells and has a large number of physiological functions in animals and plants. Ca^{2+}-CaM signaling is involved in pollen tube development (Ma et al., 1999; Rato et al., 2004), and pollen tube elongation can be inhibited by extracellular application of CaM antagonists such as trifluoperazine (TFP), calmidazolium, W-7, and W-12 (Picton and Steer, 1985; Rato et al., 2004). The CaM signaling pathways and the physiological responses that they elicit depend on the expression patterns and activities of the downstream molecules regulated by Ca^{2+}-CaM. Most previous studies have focused solely on the morphology and cytology putatively related to CaM functions. However,

the data available thus far are still insufficient to provide a complete picture of the functions of CaM during pollen tube development. TFP is a potent antipsychotic phenothiazine and has been widely studied in relation to its mode of binding and specific inactivation of CaM (Picton and Steer, 1985; Vandonselaar et al., 1994; Krinke et al., 2007). Therefore, we set up several pharmacological experiments including large-scale proteomic analysis using safe concentrations of TFP in order to extend our knowledge of the involvement of CaM in pollen tube growth.

Transcriptomic investigations have greatly enriched our insights on Arabidopsis (*Arabidopsis thaliana*) pollen development in a genome-wide range (Pina et al., 2005). However, gene expression at the transcriptional level does not always directly correlate with protein level and activity. Proteomic analyses have been conducted on several tissues involved in plant sexual reproduction, such as rice (*Oryza sativa*) anthers containing young microspores or under early cold stress and in male gametophytes at various developmental stages (Imin et al., 2001, 2004; Kerim et al., 2003), but these reports did not discriminate between gametophytic and sporophytic tissues of the anther. Studies focusing solely on the proteome of the male gametophyte have been performed in Arabidopsis and *Pinus strobus* (Fernando, 2005; Holmes-Davis et al., 2005). Recent proteomic investigations of pollens from Arabidopsis, rice, and gymnosperms have provided opportunities to complement the information derived from transcriptomic analysis and offered new insights into the mechanisms underlying pollen functional specification (Noir et al., 2005; Dai et al., 2006, 2007; Sheoran et al., 2006). However, pollen tube development in conifers (gymnosperm) differs in several ways from that in angiosperms, such as in the extended growth period, relatively slow growth rate, and extremely delayed gametogenesis, which represent a major evolutionary divergence in male gametophyte development in the flowering plants (Fernando, 2005, Fernando et al., 2005; Williams, 2008). Moreover, conifers produce abundant well-germinated pollen that can be obtained without contamination, making it ideal for proteomic research. There have been no reports, to our knowledge, on the global analysis of pollen tube proteins that focus specifically on Ca^{2+}-CaM signaling. We report here the identification of differentially expressed proteins in pollen tubes in which Ca^{2+}-CaM signaling had been blocked. These data will provide new insights into the regulation of Ca^{2+}-CaM signaling in pollen tubes.

RESULTS

### Expression Profiles of Elongating Pollen Tubes after TFP Application

Pollen germination was initiated after approximately 12 h of incubation in the standard medium and reached a maximum germination percentage of 92% after 24 h. The inhibitor TFP at a concentration of 25 μM had an evident effect on the maximum germination percentage. In the presence of 50 μM TFP, the average growth rate of pollen tubes was 8.2 μm h^{-1}. When the TFP concentration was increased to 100 μM, the average growth rate dropped to 3.6 μm h^{-1}, compared with 13.2 μm h^{-1} in the control line during 15 h of incubation. The pharmacological experiments revealed that both pollen germination and tube elongation were inhibited by TFP in a dose-dependent manner (Fig. 1; Supplemental Fig. S1).

Moreover, fluorescein diacetate and propidium iodide staining both showed that the TFP-treated pollen tubes in this study maintained cell vitality and were still growing (Supplemental Figs. S2 and S3). Another CaM antagonist, W7, exhibited similar inhibitory patterns (Supplemental Fig. S4). Total proteins were extracted from pollen tubes at 6, 12, 16, and 20 h after treatment with two concentrations of TFP (25 and 50 μM) to investigate temporal characteristics in protein variation. Reproducible protein expression profiles and nearly 800 spots were resolved on the Coomassie Brilliant Blue R-250-stained two-dimensional (2-D) gels over a pH range of 3 to 10. Most spots were around pI 4 to 8, with molecular masses from 14 to 97 kD. We also extracted total proteins at 0.5, 1, and 6 h after TFP treatment and then subjected them to proteomic analyses with dry strips of pH 4 to 7 in order to detect the early variations in protein expression profiles. Ninety-five spots responded to TFP by either up- or down-regulation, whereas the global pattern of pollen tube protein expression was largely unchanged. These differentially displayed spots were subjected to in-gel digestion and mass spectrometry. Reference maps with annotated pollen tube 2-D patterns are shown in Supplemental Figures S5 and S6, and all identified proteins are listed in Supplemental Tables S1 and S2. Selected sections of the gels were magnified to highlight the time- and dose-dependent variations in the differentially expressed proteins after the perturbation of Ca^{2+}-CaM signaling (Figs. 2 and 3). Because of the lack of genome information for conifers and the low abundance of some proteins, only 75 of the 95 spots examined were identical to those already reported in the National Center for Biotechnology Information nonredundant (NCBI nr) database by cross-species matching. The remaining 20 unidentified proteins were subjected to de novo sequencing and MS BLAST, and 18 proteins were identified. Two proteins (spots 9 and 57) were not identified in routine searches of Mascot against the NCBI nr database, whereas searches of the EST others database resulted in positive matches to existing EST sequences. Of the identified proteins, 43 were previously reported in conifers and the other 50 showed high homology to those reported in other plants (Supplemental Tables S1 and S2).

Functional Significance of the Identified Protein Categories

The 93 proteins identified represented 62 different gene products and were subsequently classified into 11 func-
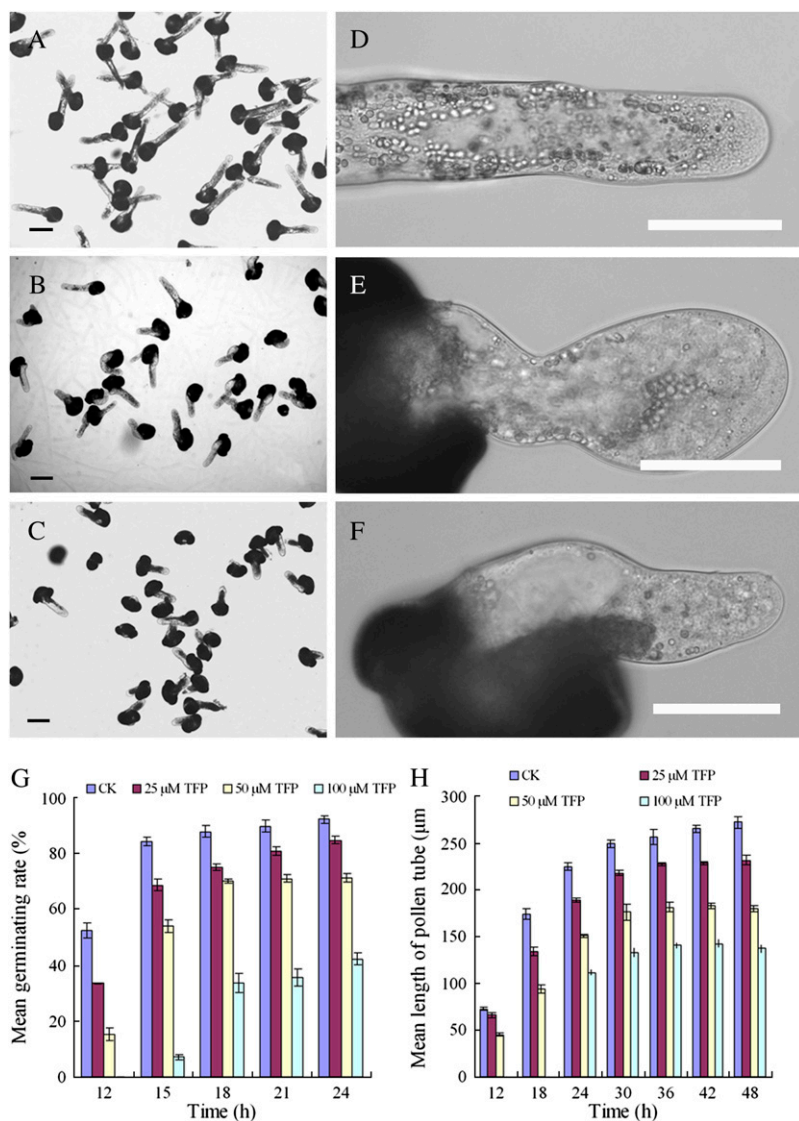
Figure 1. Inhibitory effects of TFP on pollen germination and tube morphology. Various concentrations of the inhibitor were freshly prepared in Milli-Q-grade water (the concentration of the stock solution was 5 mg mL^{-1}) and directly added to the germination medium at the beginning of the culture period. A, Healthy pollen tubes cultured in standard medium for 20 h, showing high germination rate and long pollen tubes with normal shape. B, Pollen tubes cultured in medium containing 25 μM TFP for 20 h, showing decreased germination rate and a few short tubes with morphological abnormalities. C, Pollen tubes cultured in medium containing 50 μM TFP for 20 h, showing that pollen germination was significantly inhibited. D, A pollen tube cultured in the standard medium for 20 h, showing a regularly shaped pollen tube of constant diameter and a clear zone in the apical region. E and F, Typical phenotypes of pollen tubes cultured in the presence of TFP for 20 h. E, Pollen tube incubated in 25 μM TFP, showing a twisted growth pattern. F, Pollen tube incubated in 50 μM TFP, showing obvious vacuolation and amyloplasts. Bars = 50 μm. G and H, Statistical data for the antagonizing effects of TFP on pollen germination and tube elongation. G, Inhibitory effect of TFP on pollen germination rate. Pollen germination was inhibited by TFP in a dose-dependent manner. H, Inhibitory effect of TFP on pollen tube elongation. Pollen tube elongation was inhibited by TFP in a dose-dependent manner. [See online article for color version of this figure.]

tional categories according to their putative functions using the scheme described by Bevan et al. (1998). These data emphasize the wide range of proteins related to Ca^{2+}-CaM regulation (Supplemental Fig. S7). The most abundant category was represented by energy-associated proteins (31%). The second category was classified as metabolism-related proteins (13%). Other functional categories included those for protein synthesis, transport, signal transduction, cell structure, and others. Some proteins have not previously been assigned functions in the process of pollen tube development. Mascot searches for two proteins (spots 39 and 45) found no annotated biological functions; thus, putative functions were assigned using an NCBI BLAST search.
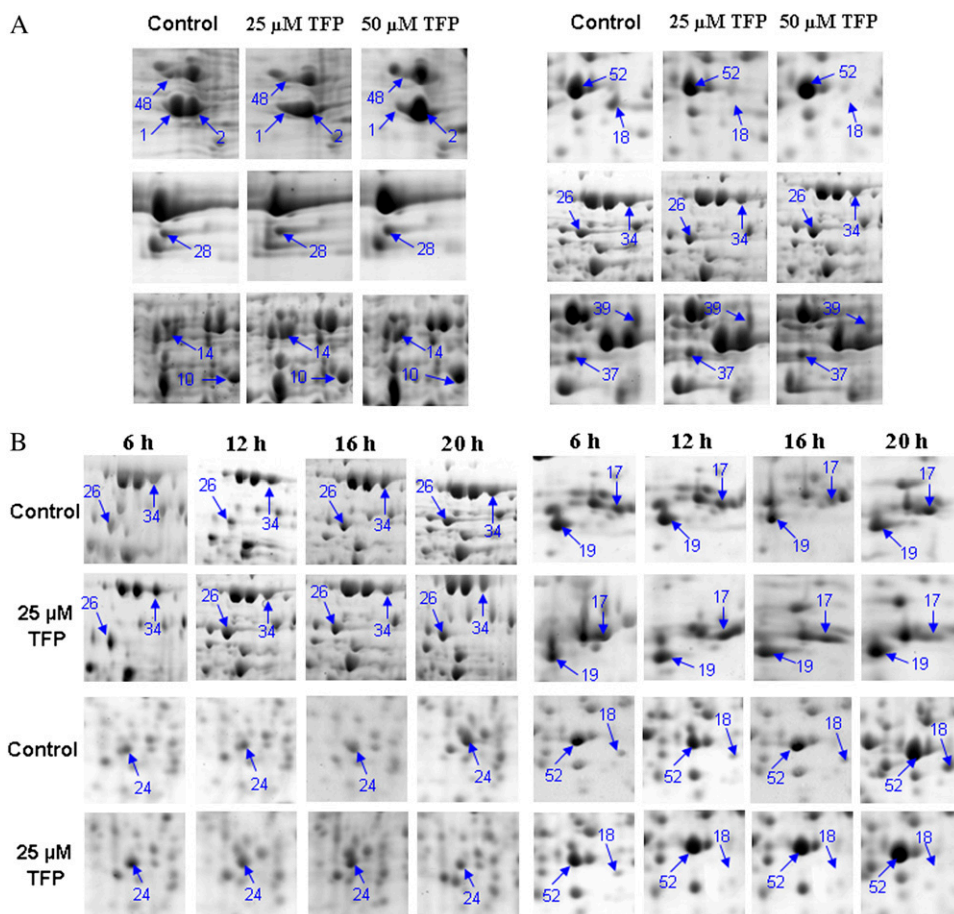
Quantitative Analysis of Proteome Patterns after TFP Treatment

To determine the proteins related to the inhibitory effect of TFP and to identify which proteins contribute to the primary/secondary responses after TFP appli-

cation, proteins were extracted at 6, 12, 16, and 20 h after treatment with TFP (25 or 50 μM) and then separated using 2-D gels to investigate dose-dependent and temporal characteristics. Proteins were also extracted after treatment with 25 μM TFP for 0.5, 1, and 6 h to detect the variations in protein expression profiles at early stages. The quantitative variations in most of the differentially expressed proteins followed strict dose dependence, with the most significant variations at a concentration of 50 μM TFP (Supplemental Tables S1 and S2). Some proteins decreased or increased steadily as the concentration of TFP increased (e.g. spots 1, 15, 16, etc.). Interestingly, some proteins were strongly induced or inhibited at low concentrations of TFP but were then maintained at a constant level, even if exposed to a high concentration of inhibitor for a longer time (e.g. spots 3, 8, 41, etc.).

Of the 93 proteins identified, 71 were differentially expressed in different patterns during time-course analysis in different developing stages after TFP treat-

Figure 2. Zoomed sections from 2-D gels to show the dose-dependent and time-dependent manner of differentially expressed proteins. Spot quantitation was performed from at least three independent gels from each total protein sample. A, Total proteins were extracted from control cells and pollen tubes cultured in the presence of 25 μM and 50 μM TFP for 16 h. B, Total proteins from control cells and treated cells (25 μM TFP) were extracted after 6, 12, 16, and 20 h of incubation. [See online article for color version of this figure.]

ment (Fig. 4). Similar to the dose-dependent changes, comparisons of proteome patterns over the prolonged time sequence revealed that 42 spots of the up-/down-regulated proteins showed quantitative variations over time at early stages (Fig. 4, A–C; Supplemental Figs. S5 and S6). Some of these proteins showed rapid quantitative changes over 50% at 0.5 to 1 h after TFP incubation (Fig. 4; Supplemental Fig. S6, spots E1, E6, E7, and E12). Other proteins showed quantitative changes at late stages (6–20 h; Fig. 4, D and E; Supplemental Fig. S5). In contrast, down-regulated proteins (spot 1) showed quantitative changes between those of control and treated cells (Supplemental Table S1) and almost disappeared in 50 μM TFP, whereas their expression did not vary significantly in the time-course analysis. The expression patterns of several protein spots were dramatically different from most other responses (Fig. 4, D and E). For example, spots 27 and 34 obviously decreased from 6 to 12 h, whereas their expression was constant with continuous TFP treatment up to 20 h. The expression of spot 35 increased until 16 h, when it peaked, and then decreased with time to 20 h (Fig. 4E).

In general, conifer pollen tubes responded to $[Ca^{2+}]_c$ elevation (see below) by up-regulation of some signaling proteins, with organelle-related proteins (i.e. mitochondria, Golgi, and endoplasmic reticulum [ER]

functions) as the primary responses, whereas proteins involved in one-carbon unit transfer reactions and RNA binding showed the secondary responses. In contrast, some proteins were down-regulated, including those involved in signaling transduction, energy production, transcription, and translation activities as the primary responses, whereas cytoskeletal, secretory pathway, and cell wall expansion proteins appeared as the secondary responses.

TFP Rapidly Induced an Increase in Extracellular Ca^{2+} Influx and Elevated Ca^{2+} Concentrations in Pollen Tube Cytoplasm

Using the vibrating electrode technique, we measured Ca^{2+} influx at the extreme apex of growing pollen tubes (Fig. 5A). The results showed that Ca^{2+} influx prevailed in the control tube apex. The mean maximal Ca^{2+} influx at the peak of the oscillations was 54.63 ± 7.84 pmol cm^{-2} s^{-1} ($n = 5$; Fig. 5A). The magnitude of Ca^{2+} influx at the extreme apex was markedly increased and then maintained at a relatively constant level upon TFP treatment at 300 s, and the mean maximal influxes at the extreme apex after TFP treatment was 93.45 ± 6.49 pmol cm^{-2} s^{-1} ($n = 5$), indicating that the net $[Ca^{2+}]_c$ derived from extracellular Ca^{2+} bulk was substantially increased.
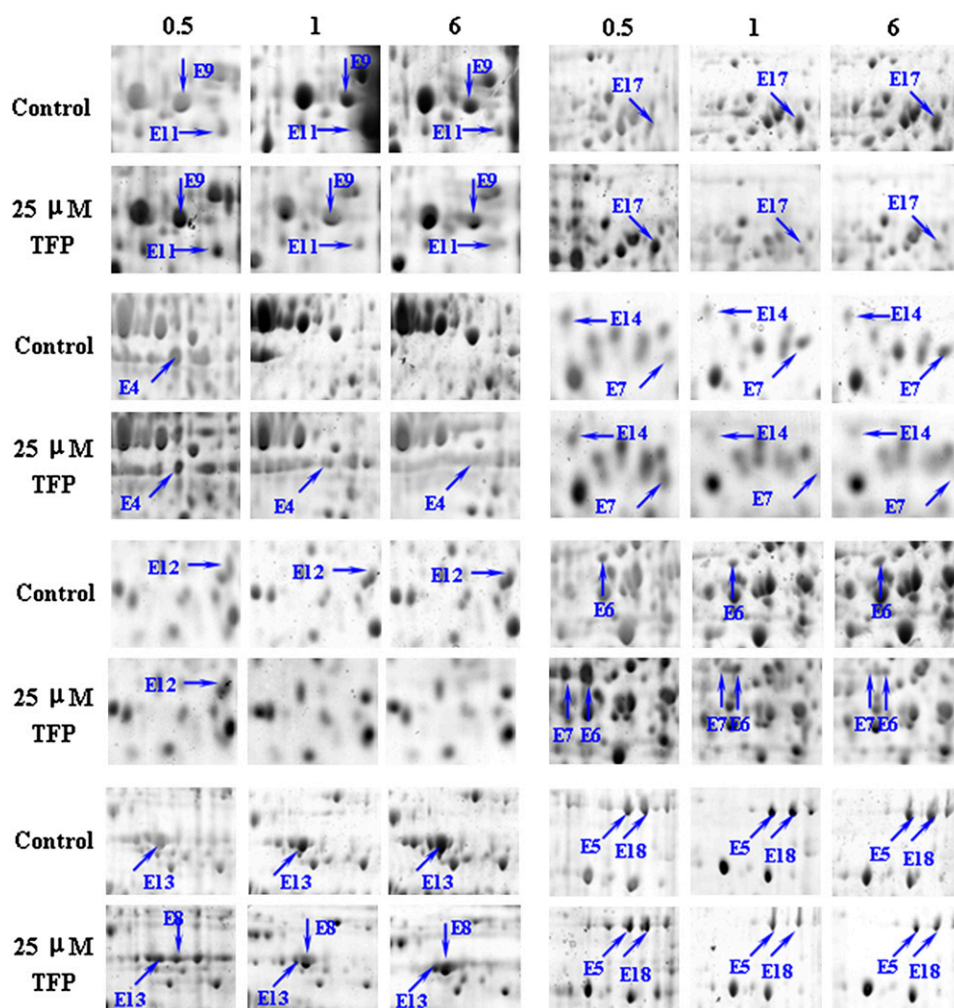
Figure 3. Zoomed sections from 2-D gels to show the time-dependent manner of differentially expressed proteins at early stages. Spot quantitation was performed from at least three independent gels from each total protein sample. Total proteins were extracted from control cells and pollen tubes cultured in the presence of 25 μM TFP. [See online article for color version of this figure.]

Furthermore, pollen tubes loaded with Fluo-3/AM showed strong intracellular fluorescence. Control pollen tubes of *Picea meyeri* displayed a typical tip-focused cytosolic Ca^{2+} gradient within 20 to 30 μm of the tip region (Fig. 5, B–D), whereas almost 80% of the pollen tubes treated with 25 μM TFP showed dissipated Ca^{2+} gradient in their tips (Fig. 5, E–G). In some (approximately 35%) pollen tubes treated with 50 μM TFP, the Ca^{2+} gradient was completely dissipated and the Ca^{2+} concentration in the tube cytoplasm increased significantly in comparison with control cells. In certain cell types, Fluo-3/AM is reported to be sequestered into vacuoles, and uneven accumulation led to the incorrect estimation of the real Ca^{2+} distribution. In this study, we used strict controls to ensure that Fluo-3/AM fluorescence is confined to the extreme tip region rather than associated with vacuoles and other organelles (Supplemental Fig. S8).

To clarify the rapid $[Ca^{2+}]_c$ elevation and the mechanism by which it is induced, lanthanum or A23187 was applied as pretreatment (Fig. 5, H–M). Lanthanum substantially inhibited the $[Ca^{2+}]_c$ elevation induced by TFP, whereas A23187 pretreatment significantly pro-

moted TFP-induced $[Ca^{2+}]_c$ elevation in the cytoplasm behind the tip region. This suggested that the rapid elevation in cytosolic Ca^{2+} resulted directly from TFP treatment and that this Ca^{2+} increase largely originated in extracellular Ca^{2+} influx via a Ca^{2+}-permeable channel. Similarly, W7 also induced a rapid increase in $[Ca^{2+}]_c$, further confirming that the elevation of $[Ca^{2+}]_c$ was a common response induced by a CaM antagonist (Supplemental Fig. S4).

Pollen Tube Ultrastructure Was Affected Early after Ca^{2+}-CaM Signaling Perturbation

Control pollen tubes examined by transmission electron microscopy had relatively electron-translucent cytoplasm filled with mitochondria, Golgi stacks, ER, lipid droplets, small vacuoles, vesicles, and starch grains (Fig. 6A). A typical transparent zone could be distinguished clearly at the tip, and larger organelles accumulated behind this clear zone. Mitochondria possessed numerous well-developed cristae and had electron-dense stroma, whereas Golgi stacks had six to eight tightly packed cisternae and were surrounded by

Short term treatment

Long term treatment
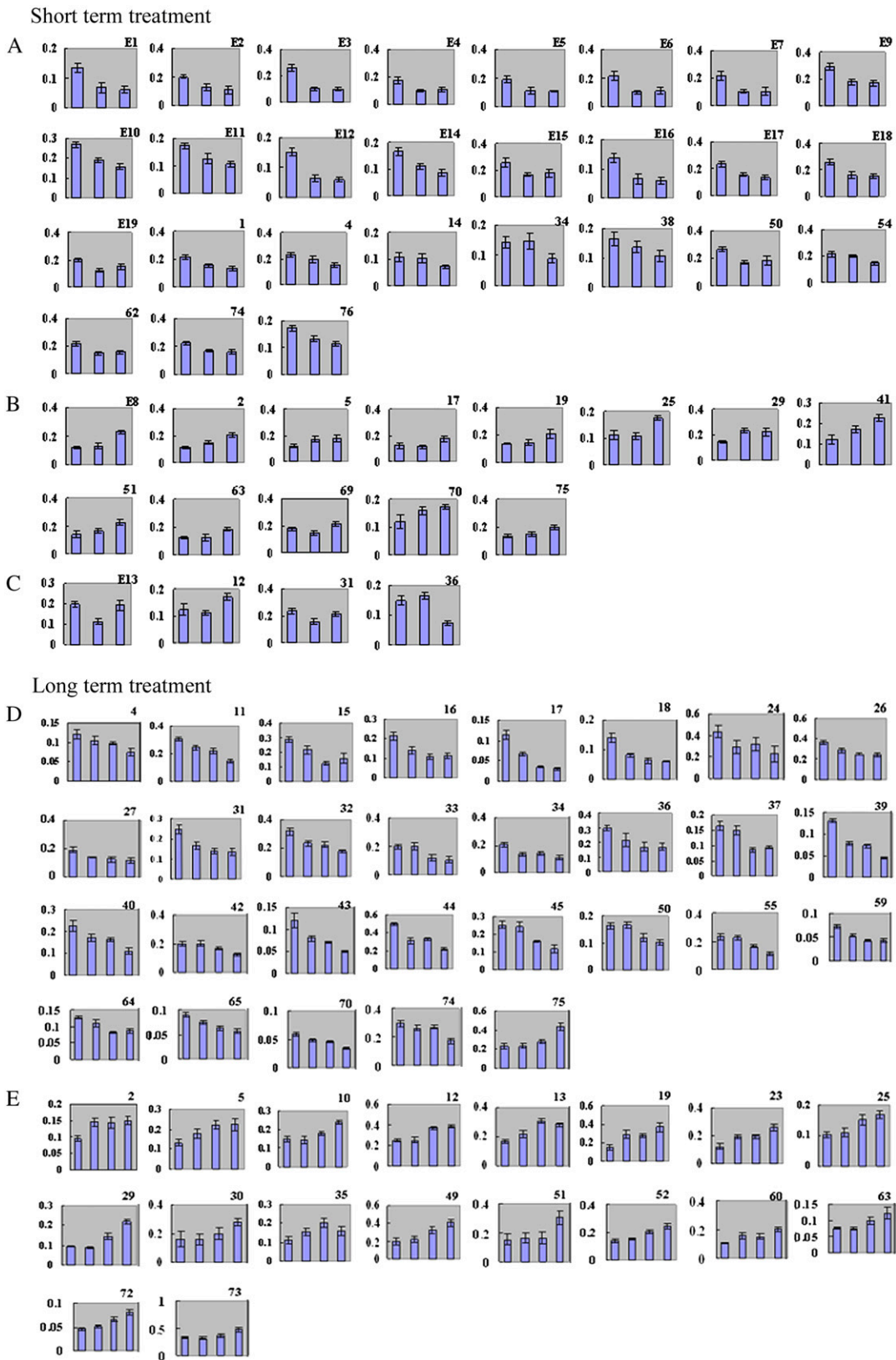
Figure 4. Histogram analysis showing relative changes in the amount of proteins determined using the ImageMaster 2D Platinum 5.0 software. Histograms indicated the time-dependent variation of proteins from pollen tubes cultured for short-term treatment (0.5, 1, and 6 h) and long-term treatment (6, 12, 16, and 20 h) in the presence of 25 μM TFP. The protein amount was

numerous secretory and coated vesicles (Fig. 6, C, E, and I). The tightly packed ER was mostly flat, with a large quantity of densely attached ribosomes (Fig. 6G).

In TFP-treated pollen tubes, the clear zone at the tip region was still distinguishable, but organelle zonation was not maintained (Fig. 6B). There were significant alterations in the organellar ultrastructure (i.e. mitochondria, Golgi stacks, and ER) as early as 1 h after inhibitor application. Mitochondria were slightly enlarged, with dramatic swelling in the cristae (Fig. 6D). Golgi cisternae (especially at the trans side) disintegrated and ruptured into vesicular structures, and ER structure was bent and fragmented, with swollen and dilated membranes (Fig. 6, F and H). The vesicle number greatly decreased in comparison with that of control cells (Fig. 6, I and J). Organellar ultrastructure did not show more severe disruption when treated with TFP for 3 or 5 h (Supplemental Fig. S9, A, C, E, G, and I). The ultrastructural abnormalities that occurred at earlier time points can be considered as primary responses induced by TFP treatment.

In contrast, long-term treatment with TFP significantly disrupted the polarized organization of the cytoplasm, and the electron-translucent zone was replaced with amyloplasts and other organelles (Supplemental Fig. S9B). Severe vacuolation of organelles and disruption of cytoplasm could only be detected following the long-term treatment. Mitochondria swelled dramatically, and the electron-dense content was severely disrupted and vacuolated (Supplemental Fig. S9, D and H). Large numbers of ribosomes were scattered throughout the cytoplasm instead of being associated with ER membranes (Supplemental Fig. S9, H and J). These ultrastructural abnormalities in the endomembrane system presumably would contribute to the breakdown of activities in the secretory pathway.

TFP Treatment Disrupted the Actin Cytoskeleton and Had Antagonistic Effects on Endocytosis/Exocytosis

In control cells, actin filaments (AFs) were distributed throughout the pollen tube in a net axial array, mainly parallel to the direction of elongation. These AFs formed a continuous network initiated from the pollen grain to the tube (Supplemental Fig. S10A). After treatment with TFP, AFs were obviously twisted and condensed, and disrupted AF fragments accumulated into clusters (Supplemental Fig. S10, B and C). The fine actin fragments observed in the tip of control cells were lost following TFP treatment.

Styryl FM dyes can be used as reliable markers of membrane trafficking events in plant cells, including

tip-growing pollen tubes and root hairs (Šamaj et al., 2005, 2006). The internalization of FM4-64 into control cells follows a strict time sequence and finally results in a typical reverse V-like staining pattern, which saturated in approximately 15 min, as indicated in the fluorospectrophotometer analysis and dynamic internalization (Fig. 7A; Supplemental Fig. S11). After treatment with TFP, the internalization process was greatly accelerated, taking approximately 9 min to reach saturation (Fig. 7B). FM4-64 fluorescence after TFP treatment could only be detected in the thin region beneath the plasma membrane, instead of the characteristic reverse V-type pattern in controls. The difference occurred only in endocytic uptake; subsequent dye redistribution was not affected. Short-term treatment with TFP for 0.5 h did not induce obvious changes in the FM4-64 staining pattern.

The extracellular activity of secreted acid phosphatase (AcPase) was assayed as a good reporter for exocytosis. A dramatic increase in AcPase activity was detected in the standard medium, especially after incubation for 18 to 24 h, which corresponded well to the period of rapid growth in pollen tubes. In comparison with control cells, AcPase activity decreased by 22.31%, 41.69%, and 33.37% in pollen tubes treated with 25 μM TFP for 18, 24, and 30 h, respectively. When the inhibitor concentration was increased to 50 μM, AcPase activity decreased by 49.29%, 56.15%, and 56.61% at 18, 24, and 30 h, respectively (Fig. 7C), indicating that the increase of AcPase in TFP-treated tubes was lower than that seen in controls. No significant variation was recorded during the first 12 h, and especially in the first 6 h, which correlated well with the growth status of the pollen tubes (Fig. 6, I and J).

Distribution/Configuration of Cell Wall Components Changed Due to Ca²⁺-CaM Dysfunction after TFP Treatment

Immunolabeling, fluorescence staining, and Fourier-transformed infrared (FTIR) microspectroscopy were used to analyze changes in cell wall components upon CaM dysfunction. After TFP application, deesterified pectins were no longer depleted from the extreme apex and could be observed along the whole length of the tube (Fig. 8, A and B), whereas esterified pectins were found only in the basal site near the germinating aperture, instead of accumulating at the tip (Fig. 8, C and D). Unlike the uniform deposition in control cells, cellulose deposition was reduced in the swollen tip region of the tube wall after inhibitor treatment (Fig. 8, E–G). TFP treatment caused arabinogalactan proteins (AGPs) to accumulate at the basal site of the pollen

---

Figure 4. (*Continued.*)
determined according to the percentage of spot volume. They were grouped according to changes during the time course. A, Down-regulated proteins in short-term treatment. B, Up-regulated proteins in short-term treatment. C, Spots did not show obvious changing tendency. D, Down-regulated proteins in long-term treatment. E, Up-regulated proteins in long-term treatment. [See online article for color version of this figure.]

Figure 5. Rapid changes in extracellular Ca^{2+} influx and $[Ca^{2+}]_c$ in response to TFP treatment. A, Noninvasive scanning ion-selective electrode measurement showed that 25 μM TFP treatment induced a rapid increase in extracellular Ca^{2+} influx and then maintained at the relatively high level. B to D, Time course of $[Ca^{2+}]_c$ in a control pollen tube, indicating a tip-focused Ca^{2+} gradient at the very tip while $[Ca^{2+}]_c$ behind the tip region was relatively low. E to G, Time course of $[Ca^{2+}]_c$ in a 25 μM TFP-treated pollen tube, showing an obviously elevated $[Ca^{2+}]_c$ in the cytoplasm, particularly behind the tip region. H to J, Pretreatment of the pollen tube with 20 μM La^{3-} for 10 min substantially inhibited the elevation in $[Ca^{2+}]_c$ induced by TFP. K to M, Pretreatment of the pollen tube with 1 μM A23187 for 10 min, showing that TFP treatment induced prominent elevation of $[Ca^{2+}]_c$ in the tube cytoplasm after the Ca^{2+} concentration across the plasma membrane was balanced. Bars = 50 μm. [See online article for color version of this figure.]

Control   TFP treatment   La³⁺ pretreatment   A23187 pretreatment
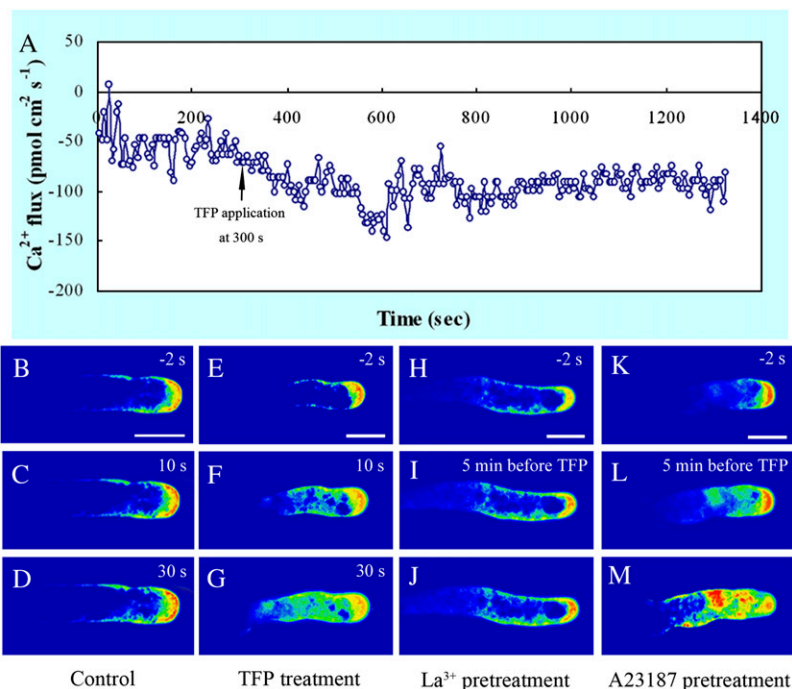
tube, instead of the characteristic periodic ring-like deposits (Fig. 8, H and I). Compared with the uniform distribution along the tube shank in controls, callose staining was random, with enhanced deposition in the tube wall of TFP-treated samples. Interestingly, many aniline blue-stained particles were found in the tube cytoplasm after TFP treatment (Fig. 8, J and K). Highly reproducible FTIR spectra further confirmed immunolocalization and histochemical data. Protein peaks at 1,650 and 1,550 cm^{-1}, a saturated ester peak at 1,740 cm^{-1}, and cellulose peaks at 1,160 and 1,080 cm^{-1} all decreased, whereas the carbohydrate stretches at 1,000 to 900 cm^{-1} substantially increased (Fig. 8, L and M). To clarify that the cytological changes in the cell wall resulted directly from the inhibitory effects of TFP, brefeldin A (BFA), a specific drug that disturbs vesicle trafficking, was used to treat pollen tubes. Under BFA influence, cell wall components displayed changes different from those after TFP treatment (Supplemental Fig. S12). Moreover, both deesterified and esterified pectins had similar distribution patterns to those after TFP treatment when the growth rates of control and treated pollen tubes were comparable (in a time frame that was earlier [e.g. 12 h versus 14 h, etc.]), demonstrating that changes in the pectin distribution resulted directly from TFP treatment rather than merely from growth inhibition.

DISCUSSION

Ca^{2+}-CaM plays an essential role in the interpretation of Ca^{2+} signatures and their transduction to the downstream signaling components by binding to and altering the activities of various enzymes as well as cytoskeletal and structural proteins (Reddy et al., 2002; Rato et al., 2004). In gymnosperm species, the initiation of germination and the maintenance of subsequent tube elongation depended on continuous protein synthesis (Fernando et al., 2001; Hao et al., 2005), in contrast to the angiosperm pollen tube growth, in which pollen grains have presynthesized a complement of proteins (Mascarenhas, 1993; Dai et al., 2007). Thus, the inhibitor was added at the beginning of incubation in order to further illustrate the continuity of protein synthesis required for pollen germination and tube elongation.

Increase in Extracellular Ca^{2+} Influx and Rapid Elevation in Cytosolic Ca^{2+} as the First Primary Response

It has been well documented that a pivotal function of CaM that operates in both plants and animals is the regulation of cytosolic Ca^{2+} level (Gilroy et al., 1987; Harper and Daly, 2000; Kaplan et al., 2006). Rato et al. (2004) reported that CaM activity in the pollen tubes exhibited a tip-focused gradient, similar to the distribution of cytosol-free calcium during the polarized growth of *Agapanthus umbellatus* and also *Lilium longiflorum*, indicating that CaM may be involved in the guidance mechanism as an important Ca^{2+} transducer. Previous investigations demonstrated that a rapid elevation of $[Ca^{2+}]_c$ occurred as an early event in serial self-incompatibility reactions of *Papaver rhoeas* pollen tubes (Geitmann et al., 2000, 2004). We found here that there was also a rapid $[Ca^{2+}]_c$ elevation within seconds after treatment. In a parallel analysis using W-7 as the CaM antagonist, we confirmed that this rapid $[Ca^{2+}]_c$
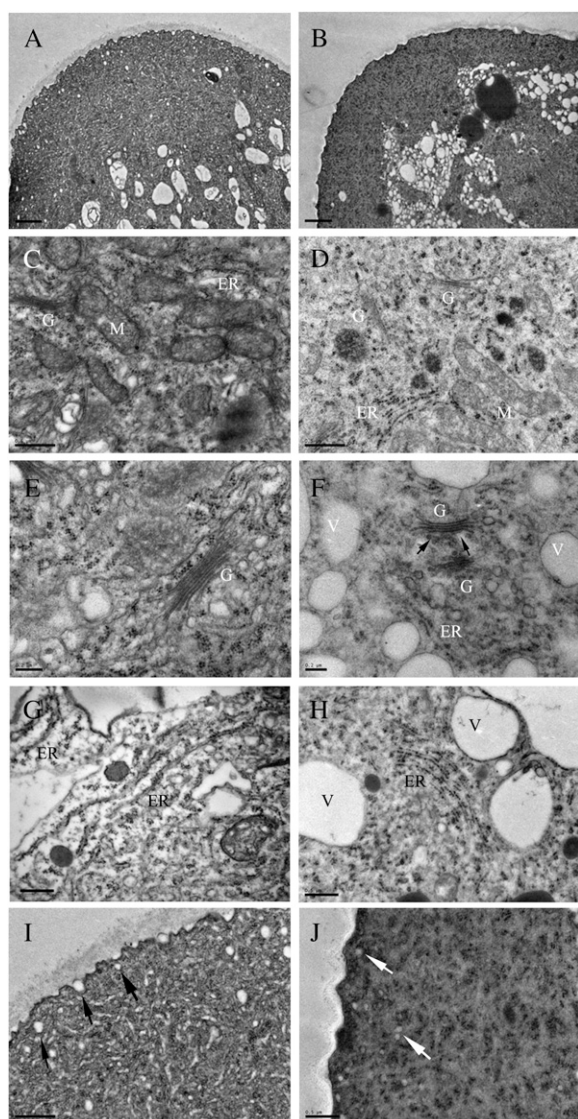
Figure 6. Organelles showing ultrastructural abnormalities as early as 1 h upon TFP treatment. A, Overview of the tip region of a control pollen tube showing the apical clear zone filled with vesicles and a subapical region containing mitochondria, Golgi stacks, and small vacuoles. Bar = 1 μm. B, Overview of the tip region in a TFP-treated pollen tube (treated with 50 μM TFP for 1 h), revealing the small vacuoles with tendency to accumulate and larger organelles such as lipid droplets appearing in the clear zone. Bar = 2 μm. C, Mitochondria in a control pollen tube with double outer membranes, dense matrix, and abundant cristae. Bar = 0.5 μm. D, Ultrastructural changes in mitochondria induced by 1 h of TFP treatment, including decreased electron density of matrix, slight enlargement of size, and disrupted cristae. Bar = 0.5 μm. E, Golgi apparatus in a control pollen tube, displaying normal ultrastructure with associated vesicles of different sizes. Bar = 0.2 μm. F, Obvious abnormalities in Golgi cisternae appeared after TFP treatment for 1 h, such as disintegrated cisternae (especially at the trans side) and lower number of cisternae. Arrows point to the disrupted cisternae. Bar = 0.2 μm. G, Rough ER in a control pollen tube showing abundant ribosomes attached to it. Bar = 0.2 μm. H, After a short-term treatment with TFP for 1 h, rough ER was disintegrated and ruptured into vesicular structures. Bar = 0.5 μm. I, Numerous vesicles accumulated at the tip region of control pollen

elevation was induced largely when TFP was used as the Ca^{2+}-CaM antagonist, similar to previous results reported in carrot (*Daucus carota*) protoplasts and intact Arabidopsis and tobacco (*Nicotiana tabacum*) seedlings (Gilroy et al., 1987; Kaplan et al., 2006). However, the results from fluorescein diacetate and propidium iodide staining showed that the TFP-treated pollen tubes maintained their vitality, indicating that the cytological events induced by TFP were not part of programmed cell death reactions. Furthermore, recovery experiments after removing TFP demonstrated that TFP-treated pollen tubes can resume the typical transparent zones and continue fast growth, indicating that the downstream cytological events were different from those after rapid [Ca^{2+}]$_c$ elevation in self-incompatibility reactions and are specific to the induction from Ca^{2+}-CaM antagonists. We propose that the rapid increase in extracellular Ca^{2+} influx and cytosolic Ca^{2+} elevation within a couple of minutes was the primary response induced by TFP treatment that triggered further downstream reactions.

Signaling Proteins as the Pleiotropic Responses

Transcriptome analysis of Arabidopsis pollen showed that the largest functional category of genes expressed contributes to signal transduction (Pina et al., 2005). Our time-course analysis of protein expression revealed that signaling proteins were differentially regulated at different stages. Most of the signaling proteins (seven proteins) showed significant quantitative variations as the primary responses. Calreticulin (spots 1, 2, and 48) was the most potent protein in Ca^{2+}-binding capacity identified (Krause and Michalak, 1997), and its overexpression leads to an increase of Ca^{2+} in the ER and simultaneous depletion in the cytoplasmic signaling pool (Persson et al., 2001). We can safely conclude that the dramatically elevated Ca^{2+} concentrations in the cytoplasm correlated well with the strong down-regulation of calreticulins (spots 1 and 48). In addition, the newly identified Hyp-rich glycoprotein (spot E17) is a stress-responsive lectin-like protein that contains a QXW lectin repeat domain, which might be a first step in the recognition of the involvement and importance of protein-glycoconjugate interactions in some essential cellular processes (Wu et al., 2001; Fouquaert et al., 2008).

Porins and porin-like proteins (spots 18, 19, 43, and 76) are voltage-gated anion channels that are localized in the outer membrane of mitochondria. Hill et al. (2000) observed porin-like activities mediated by Ca^{2+} signaling during the response of *Spermatozopsis similis* to photoshock and mechanoshock. Since the dominant porin was highly permeable to Ca^{2+} and acts as a transducer in Ca^{2+} signaling modulation, we conclude that

tubes. Some of them were connected to the plasma membrane at the very tip. Arrows indicated single vesicles in the tip region. Bar = 0.5 μm. J, Vesicles dramatically decreased in the tip region. Bar = 1 μm. G, Golgi stack; M, mitochondria; V, vacuole.

Figure 7. Endocytosis was promoted while exocytotic activity decreased after TFP treatment. Pollen tubes were incubated in the standard medium and medium containing 25 μM TFP for 16 h and then were subjected to FM4-64 staining. A, FM4-64 internalization started after incubation for about 7 min, and saturation was completed at about 15 min. Finally, FM4-64 displayed a reverse V-like staining pattern in the control tube. Bar = 50 μm. B, FM4-64 internalization started immediately after dye application, and the dye saturation was achieved at 9 min. Finally, FM4-64 accumulated in a small region under the plasma membrane. Bar = 50 μm. C, AcPase activity elevation was detected in the standard medium, especially at 18 to 24 h after incubation. This enzyme activity was inhibited in a dose-dependent manner. D, Corresponding positions of FM4-64 fluorescence, vacuoles (V), and starch grains (S) in the cytoplasm of control and TFP-treated pollen tubes. Bar = 50 μm. The region marked from the straight lines to the extreme tip corresponded to the so-called clear region without large organelles and starch grains. [See online article for color version of this figure.]
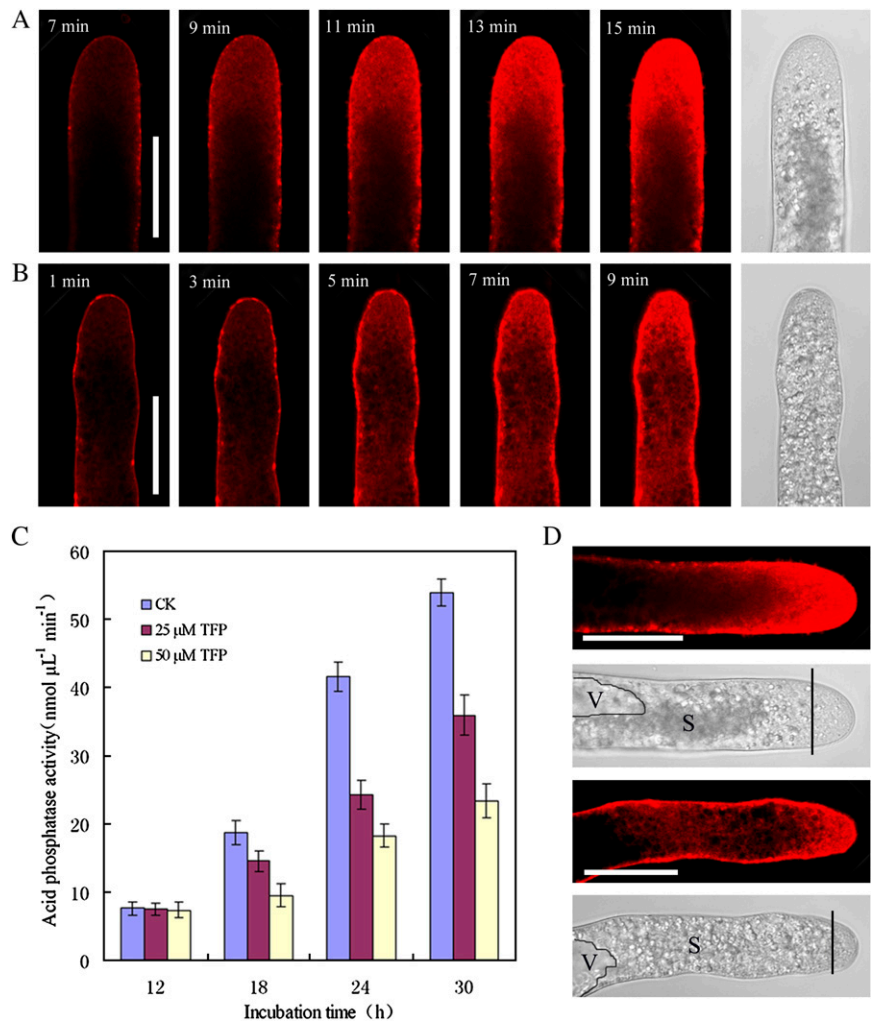
the identified porins in pollen tubes may function in ion homeostasis maintenance during Ca^{2+} signaling and concentration balancing.

Another up-regulated protein was matched as nucleoside diphosphate kinase B (spot 58), which is a key enzyme in maintaining the cellular balance of nucleoside triphosphates (Parks and Agarwal, 1973). Previous studies revealed that nucleoside diphosphate kinase B could serve both as a guanine nucleotide exchange factor and as a GTPase-activating protein (Knorpp et al., 2003). This result indicates that activated components of the G-protein signaling pathway are likely involved in the primary response mediated by signaling proteins.

In contrast to most signaling proteins that varied as primary responses, some signaling proteins displayed differential expression patterns as important components of the secondary responses. For example, proteasome α-subunit-like protein (spot 75) was significantly up-regulated until 20 h after treatment. This protein is involved in the degradation of intracellular protein bulk in eukaryotic cells, including misfolded proteins and short- and long-living regulatory proteins. The up-regulation of this protein at a later time point suggested that the ubiquitin/proteasome pathway was activated due to the accumulation of misfolded proteins and heat shock proteins.

Proteins Involved in Energy Production and Organellar Function as the Primary Responses

Since growing pollen tubes respire at least 10 times faster than green leaf tissue (Tadege et al., 1999), tip growth poses distinct demands on energy production and biosynthetic capacity. Among the identified proteins, three general categories containing enzymes of central metabolic pathways were found, all of which were involved in energy production (Supplemental Fig. S13, marked in red).

The first subcategory consists of 12 enzymes involved in general energy production. It contains 10 key and rate-limiting enzymes involved in glycolysis (phosphoglycerate kinase, enolase, triosephosphate isomerase, glyceraldehyde-3-phosphate dehydrogenase, Fru-1,6-bisphosphate aldolase; spots 9, 15, 16, 24, 32, 33, 39, 56, 72, and 74) and four enzymes of the citrate cycle (aconitate hydratase, malate dehydrog-
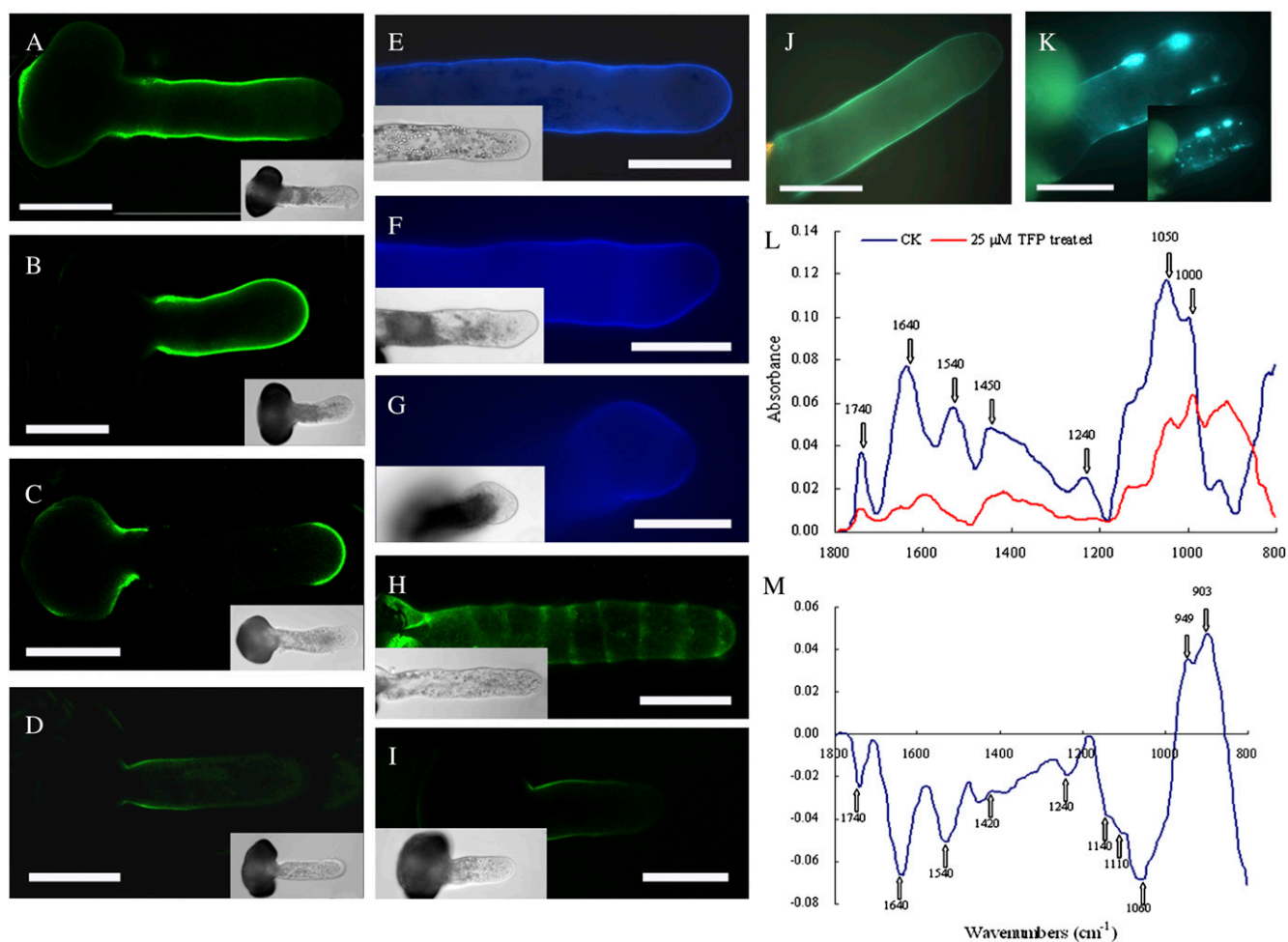
Figure 8. Immunolocalization, histochemical staining, and FTIR analysis of cell wall components. Pollen tubes were incubated in the standard medium and medium containing 25 μM TFP for 16 h and then were subjected to pectin, cellulose, AGP, and callose staining as well as FTIR analysis. A, Deesterified pectins occurred along the entire pollen tube wall except the tip region. B, JIM5 labeling of pollen tubes treated with 25 μM TFP, showing that fluorescence occurred all along the cell wall. C, JIM7 labeling of control pollen tubes. The esterified pectins localized in the extreme tip region of pollen tubes. D, JIM7 labeling of pollen tubes treated with 25 μM TFP. The esterified pectins were accumulated at the basal part of the pollen tube wall. E, Cellulose distributed throughout the tube wall in the control pollen tube, including the elongating tip. F and G, After treatment with 25 μM TFP, pollen tubes showed less cellulose than in control cells, especially at the extreme apex (F). In some pollen tubes, the cellulose layer could only be ambiguously discerned in the extreme apex (G). H, Pollen tubes incubated in standard medium exhibiting a characteristic ring-like pattern of AGP distribution along the whole length after staining with LM2 antibodies. I, Pollen tube cultured in the presence of 25 μM TFP. Note that the fluorescence could only be found in the shank of pollen tubes instead of the characteristic ring-like deposition. J, Pollen tubes cultured in the standard medium displaying regularly distributed fluorescence along the tube shank when stained with decolored aniline blue. The fluorescence in the tip region was difficult to detect. K, Pollen tubes cultured in the presence of 25 μM TFP, showing numerous small particles in the cytoplasm and some of them fused with the cell wall. A different focusing plane was shown in small size, showing stained particles in the cytoplasm. Corresponding bright-field images are shown in the insets. Bars = 50 μm. L, FTIR spectra of cell wall components in a control tube and a 25 μM TFP-treated tube. M, Differential spectrum generated by digital subtraction of spectrum of a 25 μM TFP-treated tube from that of a control pollen tube. [See online article for color version of this figure.]

enase/oxidoreductase, pyruvate dehydrogenase E1 β-subunit isoform 2; spots 34, 44, 45, and 53) that regulate carbon flow and energy production. The gradual down-regulation of these enzymes of the main energy-producing pathways indicates that their metabolic levels were generally reduced after TFP treatment. Thus, ATP production from glycolysis and

the citrate cycle was inhibited and contributed to arrested pollen germination and tube elongation.

The second subcategory consists of six enzymes that are directly involved in oxidative phosphorylation and ethanol fermentation. All of the three critical mitochondrial enzymes involved in ethanol fermentation were found in gymnosperm pollen tubes: pyruvate

decarboxylase (PDC; spot 28), aldehyde dehydrogenase (spots 6, 14, 61, and E18), and alcohol dehydrogenase (spots E11 and 41) were up-regulated, whereas the mitochondrial ATP synthase β-subunit (spot 4) was down-regulated. The down-regulation of the mitochondrial ATP synthase β-subunit, together with proteins from the first subcategory, indicates repressed ATP production from the main metabolic and energy-producing pathways, whereas the up-regulation of PDC and aldehyde dehydrogenase may promote energy production by ethanol fermentation. Actually, PDC bypass provides growing pollen tubes with a competitive advantage under low-oxygen conditions, when energy production from oxidative phosphorylation is impaired (Mellema et al., 2002; Gass et al., 2005).

Cytologically, dramatic changes of mitochondria, Golgi stacks, and ER together with a significant decrease in the number of secretory vesicles were observed as early as 1 h after TFP treatment. These substantial alterations showed similarities to the swelling of mitochondria and/or rupture of their cristae described for several animal systems and the self-incompatible system in *P. rhoeas* pollen tubes (Korichneva and Hammerling, 1999; Geitmann et al., 2004), indicating subsequent potential alterations in the secretory activities maintained by the endomembrane system. In contrast, severe vacuolation of organelles (namely mitochondria and ER) and disruption of the cytoplasm could only be detected after long-term TFP treatment, indicating that the vacuolation/disruption of organelles/cytoplasm may appear as secondary alterations following the primary changes.

Proteins Involved in Cellular Structure/Secretory Pathway as the Secondary Responses

It has been reported that G-actin expression decreased steadily and that the ultrastructure of organelles was also affected by prolonged latrunculin B treatment (Chen et al., 2006), whereas nonspecific inhibition by high turgor pressure did not result in similar effects on actin rearrangement (Chen et al., 2007). Here, we detected the gradual down-regulation of actin after CaM dysfunction and $[Ca^{2+}]_c$ elevation, which was consistent with previous investigations of Ca^{2+}-CaM regulations on the F-actin-binding activity of a 135-kD actin-bundling protein (Yokota et al., 2000). We also found one down-regulated protein that corresponded to a myosin-like protein (spot 68) after TFP treatment, which is a crucial motor protein involved in directing vesicle/organelle transport via the force-generating hydrolysis of ATP (Cheung and Wu, 2004; Staiger and Hussey, 2004); its down-regulation indicates potential deficiencies in actomyosin-directed cargo transport. The inhibitor-induced actin remodeling was related to the increased cytosolic $[Ca^{2+}]_c$ rather than a result of growth inhibition, and the elevation of cytosolic Ca^{2+} led directly to the breakdown of fine AFs/myosin guidance, followed by changes in vesicle trafficking and mitochondrial distribution.

The up-regulation of mitochondria-localized low-molecular-weight heat shock protein (spot 60) and luminal binding protein (BiP; spots 25 and 30) can lead to the accumulation of these chaperones in the mitochondria/ER lumen and to protein-folding defects, whereas the down-regulation of calreticulin will cause the accumulation of misfolded proteins that cannot escape from the ER. Both alternatives ultimately result in ER swelling and the other ultrastructural changes that we observed. In addition to BiPs and calreticulins, the down-regulation of putative mitochondria processing peptidase α-subunit (spot 31) and the up-regulation of disulfide isomerase precursor (spots 29 and 71) are closely related to protein stabilization, and their differential expression may be a direct reflection of the altered physiological status of organelles after TFP treatment.

Interestingly, FM4-64 staining of TFP-treated pollen tubes showed that dye internalization was accelerated in comparison with control cells. Alternative energy-producing machinery may be induced to some degree upon a Ca^{2+}-CaM signaling deficiency that allows FM endocytic uptake, in accordance with an up-regulated PDC bypass as the energy source for FM internalization (Parton et al., 2001; Gass et al., 2005). In contrast, accumulating evidence has confirmed that the dissipation of the tip-focused Ca^{2+} gradient may contribute to the decrease in vesicle accumulation and fusion (Roy et al., 1999). We found a gradual decrease in AcPase activity and a differential display of secretory pathway-related proteins (spots 12 and 57), providing direct evidence for reduced exocytic vesicular trafficking in TFP-treated pollen tubes.

Proteins Involved in Polysaccharide Synthesis as the Tertiary Responses

It is well accepted that Ca^{2+} has a profound effect on the oriented transport of vesicles toward the cell wall in the extreme pollen tube tip (Roy et al., 1999). Rapid turnover of the intracellular pool of UDPG has been reported during pollen tube elongation, which attests to the metabolic specialization of pollen tubes for rapid wall synthesis (Gibeaut, 2000).

Two different subclasses of metabolic enzymes involved in cell wall construction were down-regulated. One subclass is involved in cell wall synthesis, including UDP-Glc pyrophosphorylase (UDPase; spot 37), UDP-glucose dehydrogenase (UGDH; spot 46), reversibly glycosylated polypeptides (spots 42 and 55), and type IIIa membrane protein cp-wap13 (spot 21). The other subclass functions in cell wall remodeling (e.g. an esterase/lipase [spot 57]). Reversibly glycosylated polypeptides (spots 21, 42, 55, and 67) have been implicated in polysaccharide biosynthesis and may function in cell wall construction and starch synthesis in plants (Langeveld et al., 2002).

The down-regulation of UGDH, UDPase, and reversibly glycosylated polypeptides, all using UDPG as a precursor or sugar residue donor, suggested a general reduction in the cell wall synthesis and potential changes in cell wall components. In remodeling of the cell wall in the tip region, a nonspecific esterase/lipase is secreted into the extracellular medium and functions in the process of wall softening (Yoshida et al., 2005); its down-regulation indicated decreased activity in the continuous process of cell wall softening and a consequent increase in cell wall rigidity. Our proteomic data further confirm that the cell wall of gymnosperm pollen tubes undergoes dramatic remodeling during the perturbation of Ca^{2+}-CaM signaling. Given that mechanical characteristics of the cell wall are important for sustained polarized growth, results from fluorescence staining and FTIR analysis of cell wall components such as pectins, AGPs, callose, and cellulose confirm that the cell wall at the tip underwent dramatic remodeling and that these changes can partly be attributed to the subsequent growth arrest (Fig. 1).

Proteins Involved in Defense and Stress Responses

The dramatic increase in the proportion of proteins involved in defense and stress responses in *P. meyeri* pollen tubes is likely related to the extended period of growth of gymnosperms (Fernando, 2005; Holmes-Davis et al., 2005). We identified two important protein spots involved in stress responses (peptidylprolyl isomerase/cyclophilin and ascorbate peroxidase; spots 12 and 52). Although the most important function of ascorbate peroxidase is protection from photooxidative damage by scavenging reactive oxygen species, evidence is accumulating for its occurrence in nonphotosynthetic cells such as root nodules and tubers (Shigeoka et al., 2002). The up-regulation of ascorbate peroxidase and cyclophilin indicates that the extracellular secretion of these two proteins is blocked and that they probably accumulate within the ER, which correlates well with the acid phosphatase activity assay that showed significant inhibition of exocytic activities.

In conclusion, our sequential proteomic and cytological analyses provide further insight into the intricate regulation of Ca^{2+}-CaM in pollen tube development under conditions of TFP treatment to perturb Ca^{2+}-CaM signaling. Two novel findings are as follows: (1) rapid elevation of $[Ca^{2+}]_c$ and ultrastructural abnormalities in organelles as primary cytological responses that subsequently triggered secondary and tertiary alterations; and (2) perturbation of Ca^{2+}-CaM signaling leading to time-dependent changes in protein expression together with the serial cytological alterations. Collectively, these results substantially contribute to a deeper understanding of Ca^{2+}-CaM functions in gymnosperm pollen tube development in terms of interactions with signaling, energy-producing pathways, and cell expansion mechanism.

MATERIALS AND METHODS

Plant Material and Growth

Picea meyeri pollen grains were collected in the Botanical Garden of the Institute of Botany, Chinese Academy of Sciences, and stored at –20°C until use. Pollen grains were kept at room temperature for 30 min and then suspended in the germination medium containing 12% Suc, 0.01% H_3BO_3, and 0.01% $CaCl_2$ at pH 6.8 as documented previously (Sheng et al., 2006). All of the samples were incubated on a shaker (121 rpm) at 24°C in the dark. They were considered germinated only when the tube length was longer than the grain diameter. TFP (Sigma-Aldrich) and W-7 [*N*-(6-aminohexyl)-5-chloro-1-naphthalene sulfonamide; Calbiochem] were selected for the pharmacological treatments, and various concentrations of these two inhibitors were freshly prepared in Milli-Q-grade water (the concentrations of the stock solutions were 5 mg mL^{-1} and 5 mM, respectively); they were directly added to the germination medium at the beginning of the culture period unless otherwise mentioned.

Extraction of Pollen Tube Proteins

Pollen tubes were incubated in standard medium and medium containing 25 or 50 μM TFP for different times. The pollen tubes were sieved using a stainless-metal filter mesh (about 50 μm mesh diameter) to exclude ungerminated pollen grains, and then they were immediately subjected to grinding in liquid nitrogen. Total proteins were extracted using a modified TCA-acetone precipitation method as described previously (Chen et al., 2006). The protein concentration was determined using the Bradford method (Bradford, 1976). It has been confirmed that the slowing and stopping of growth are associated with changes in ribosome status (Capkova et al., 1994); thus, four time points (6, 12, 16, and 20 h) in the rapid growing stage were selected for the proteomic analysis according to the standard growth curve of *P. meyeri* pollen tubes.

2-D Gel Separation

2-D electrophoresis was performed using the Ettan IPGphor II isoelectric focusing system and the Ettan DALTsix system (Amersham Bioscience) as described (Chen et al., 2006). Coomassie Brilliant Blue-stained gels were scanned at 300 dots per inch using the UMAX Astra-2400S scanner (UMAX Technology) and then analyzed with ImageMaster 2D Platinum 5.0 software (Amersham Bioscience) according to the user's manual. Detailed information for the procedures of proteomic analysis is given in Supplemental Materials and Methods S1.

In-Gel Digestion and Electrospray Ionization-Tandem Mass Spectrometry Analysis

Spots were excised and subjected to in-gel trypsin digestion as described (Chen et al., 2006), desalted with ZipTip C18 (Millipore), and analyzed by ESI-Q time of flight-tandem mass spectrometry (MS/MS; Micromass). Database searching was performed using the Mascot search engine (www.matrixscience.com). To qualify as positive identification, the following criteria were used: database, NCBI nr; taxonomy, Viridiplantae (green plants); one missed cleavage was allowed; peptide tolerance, 1.2; MS/MS tolerance, 0.5; enzyme, trypsin; modifications (such as carbamidomethyl and oxidation) were used. Tandem mass spectra acquired on the electrospray ionization-quadrupole time of flight-MS/MS system were translated de novo using Peaks Studio software. Multiple sequence candidates were allowed per each interpreted tandem mass spectrum, and peptide sequences were not necessarily complete. All candidate sequences were merged into a single search string. MS BLAST searches were performed against a nonredundant protein database (nrdb95 clean) at http://genetics.bwh.harward.edu/msblast/ under default settings.

Measurement of Extracellular Ca^{2+} Influx

Pollens were incubated in the standard medium for 16 h and then collected for the analysis. Net Ca^{2+} flux was measured by Xu-Yue Science & Technology Co. (www.xuyue.net) using the noninvasive, scanning ion-selective electrode technique as described previously (Shabala et al., 2000). The data obtained by the ion-selective probe technique were analyzed with Excel spreadsheet to

convert data from the background –mV estimation of concentration and microvolt difference estimation of the local gradient into specific ion influx (pmol cm^{-2} s^{-1}).

Fluo-3/AM Loading and Confocal Imaging of Cytoplasmic [Ca^{2+}]$_c$

Fluo-3/AM ester was loaded into pollen tubes at low temperature in the dark at a final concentration of 10 μM as described. After 2 h of incubation, the pollen tubes were washed with standard medium several times and placed under room temperature for 1 h (Zhang and Renzel, 1998). The samples were mounted and photographed with a Zeiss LSM 510 META confocal laser-scanning microscope (excitation at 488 nm and emission at 515 nm). To confirm that CaM antagonists induce a common cytosolic Ca^{2+} elevation, another CaM antagonist, W-7, was chosen to examine its antagonistic effects on pollen tube development and cytosolic Ca^{2+} dynamics. In addition, a Ca^{2+} channel blocker, lanthanum, and an ionophore, A23187, were applied as control pretreatments to identify the mechanism of rapid [Ca^{2+}]$_c$ elevation.

Fluorescence Labeling of F-Actin

Pollen tubes were collected as mentioned above and then fixed in 4% paraformaldehyde in 50 mM PIPES buffer (pH 6.9), and F-actin labeling was performed with 0.2 mM TRITC-phalloidin in phosphate-buffered saline for 1 h and then rinsed as described (Chen et al., 2006). The samples were mounted on slides in 50% glycerol and examined using a confocal laser-scanning microscope with a rhodamine filter set (excitation at 514 nm). All images were projected along the z axis.

Endocytosis/Exocytosis Activity Analysis

FM4-64 loading was achieved by direct application to the growing pollen tubes to a final concentration of 5 μM as described (Parton et al., 2001). Serial optical sections were performed every 20 s for about 60 images at 1 to 2 min after dye application until the fluorescence came into saturation. Data were processed with LSM 5 software. After 16 h of culture, the pollen suspensions were supplemented with 2 μM FM4-64 for 12 min and then washed three times with standard medium. Cell-associated fluorescence was quantitated by fluorimetry using an F-4500 fluorospectrometer (Hitachi). FM4-64 was excited at 514 nm (5-nm band pass), and emission was detected at 580 nm (5-nm band pass). Cell-associated fluorescence was normalized to the cell-associated fluorescence of control pollen tube labeling, and the results of three measurements were averaged.

AcPase (EC 3.1.3.2) activity was determined as described by measuring the extracellular release of p-nitrophenol from p-nitrophenyl phosphate (Ibrahim et al., 2002). Samples collected from the culture medium at 0, 6, 12, 18, 24, or 30 h were centrifuged at 14,000 rpm for 30 min at 4°C. An appropriate volume of the supernatant was incubated with a reaction buffer containing 50 mM acetate buffer (pH 5.0), 10 mM p-nitrophenyl phosphate, and 10 mM MgCl$_2$ for 45 min at 30°C. The reaction was stopped by the addition of 100 μL of 500 mM borate buffer, and the concentration of p-nitrophenol was determined at a wavelength of 405 nm (DU 640; Beckman). All assays were performed in triplicate. Phosphatase activity was expressed as nanomoles of substrate hydrolyzed by per microliter of sample per minute.

Electron Microscopy

Pollen tubes were collected after incubation for 1, 3, and 20 h and then fixed in 2.5% glutaraldehyde in 100 mM phosphate buffer (pH 7.2) containing 2% (w/v) Suc for 2 h. Afterward, they were washed with 100 mM phosphate buffer, postfixed with 2% osmium tetraoxide for 2 h, dehydrated in an ethanol series, and finally embedded in Spurr's resin. Sections were cut using an LKB-V ultramicrotome, stained with 2% (w/v) uranyl acetate in 70% (v/v) methanol and 0.5% lead citrate, and examined with a JEM-1230 electron microscope (JEOL). In order to test the inhibitory effects of TFP in a temporal sequence, germinated pollen tubes were treated with 50 μM TFP for 1, 3, and 5 h.

Pectin Immunolabeling

Immunolabeling of pectins in the cell wall was carried out with JIM5 or JIM7 antibody as described (Derksen et al., 1999). Pollen tubes that had been incubated for 16 h were collected and then fixed in 3% p-formaldehyde in PME buffer (50 mmol L^{-1} PIPES, 0.5 mmol L^{-1} MgCl$_2$, and 1 mmol L^{-1} EGTA, pH 6.8) for 30 min at room temperature. After rinsing with PME buffer, the specimens were incubated for 2.5 h at room temperature with either JIM5 or JIM7 antibody. After incubation, pollen tubes were washed with PME buffer, incubated with fluorescein isothiocyanate-labeled sheep anti-rat IgG (ICN ImmunoBiologicals) diluted 1:100 for at least 2 h at room temperature, washed with PME buffer three times, mounted, and photographed (excitation at 488 nm and emission at 522 nm). Controls were prepared by omitting the primary antibody.

AGP Immunolabeling

Immunolabeling for AGPs followed the procedure of pectin labeling, except using LM2 as the primary antibody.

Localization of Callose and Cellulose

Pollen tubes were collected as mentioned above and subjected to aniline blue staining and calcofluor staining (Lazzaro et al., 2003; Wang et al., 2003). The samples were photographed with a Zeiss Axioskop 40 microscope (excitation filter BP395-440, chromatic beam splitter FT460, barrier filter LP470 for callose detection; excitation filter BP365, chromatic beam splitter FT395, barrier filter LP420 for cellulose detection).

FTIR Analysis

Pollen tubes were collected as mentioned above and then subjected to FTIR analysis with a MAGNA 750 FTIR spectrometer (Nicolet) as described (Wang et al., 2003). Spectra were obtained at a resolution of 8 cm^{-1}, with 128 coadded interferograms, and normalized to obtain relative absorbance.

Supplemental Data

The following materials are available in the online version of this article.

Supplemental Figure S1. The effects of exogenous CaM and TFP treatment on pollen germination and tube elongation.

Supplemental Figure S2. Fluorescein diacetate staining and propidium iodide staining of TFP-treated pollen tubes.

Supplemental Figure S3. Recovery experiments demonstrated that TFP-treated pollen tubes in this study were still alive.

Supplemental Figure S4. W7 induced a rapid increase in [Ca^{2+}]$_c$ and inhibited pollen tube elongation.

Supplemental Figure S5. Reference 2-D map for pollen tube proteins from P. meyeri.

Supplemental Figure S6. Reference 2-D map for differentially expressed pollen tube proteins at early stages.

Supplemental Figure S7. Assignment of the identified proteins to functional categories.

Supplemental Figure S8. Fluo-3/AM fluorescence was specifically associated with a tip-focused Ca^{2+} gradient rather than sequestered into and accumulated in the vacuole.

Supplemental Figure S9. Vacuolation and disruption of the organelles and cytoplasm appeared as secondary alterations following the primary response.

Supplemental Figure S10. TFP induced significant alterations in AF distribution in pollen tubes.

Supplemental Figure S11. Fluorospectrophotometer analysis of FM4-64 internalization along the entire time course.

Supplemental Figure S12. Changes in distributions of AFs, pectins, callose, and cellulose after treatment with 5 μg mL^{-1} BFA.

Supplemental Figure S13. Graphical analysis of putative functions of several identified proteins involved in metabolism and energy production.

Supplemental Table S1. Detailed information for protein identification.

Supplemental Table S2. Detailed information for identified proteins at early stages.

Supplemental Materials and Methods S1. Procedures for sample preparation and mass spectrometry.

ACKNOWLEDGMENTS

LITERATURE CITED

Bevan M, Bancroft I, Bent E, Love K, Goodman H, Dean C, Bergkamp R, Dirkse W, Van Staveren M, Stiekema W, et al (1998) Analysis of 1.9 Mb of contiguous sequence from chromosome 4 of *Arabidopsis thaliana*. Nature **391:** 485–488

Bradford MM (1976) A rapid and sensitive method for quantitation of microgram quantities of protein utilizing the principle of protein-dye-binding. Anal Biochem **72:** 248–254

Capkova V, Zbrožek J, Tupy J (1994) Protein synthesis in tobacco pollen tubes: preferential synthesis of cell-wall 69-kDa and 66-kDa glycoproteins. Sex Plant Reprod **7:** 57–66

Chen T, Teng NJ, Wu XQ, Wang YH, Tang W, Šamaj J, Baluška F, Lin JX (2007) Disruption of actin filaments by latrunculin B affects cell wall construction in *Picea meyeri* pollen tube by disturbing vesicle trafficking. Plant Cell Physiol **48:** 19–30

Chen Y, Chen T, Shen S, Zheng M, Guo Y, Lin J, Baluska F, Samaj J (2006) Differential display proteomic analysis of *Picea meyeri* pollen germination and pollen tube growth after inhibition of actin polymerization by latrunculin B. Plant J **47:** 174–195

Cheung AY, Wu HM (2001) Pollen tube guidance: right on target. Science **293:** 1441–1442

Cheung AY, Wu HM (2004) Over-expression of an *Arabidopsis* formin stimulates supernumerary actin cable formation from pollen tube cell membrane. Plant Cell **16:** 257–269

Cheung AY, Wu HM (2008) Structural and signaling networks for the polar cell growth machinery in pollen tubes. Annu Rev Plant Physiol Plant Mol Biol **59:** 547–572

Dai SJ, Chen TT, Chong K, Xue YB, Liu SQ, Wang T (2007) Proteomic identification of differentially expressed proteins associated with pollen germination and tube growth reveals characteristics of germinated *Oryza sativa* pollen. Mol Cell Proteomics **6:** 207–230

Dai SJ, Lei L, Chen TT, Chong K, Xue YB, Wang T (2006) Proteomic analyses of *Oryza sativa* mature pollen reveal novel proteins associated with pollen germination and tube growth. Proteomics **6:** 2504–2529

Derksen J, Li Y, Knuiman B, Geurts H (1999) The wall of *Pinus sylvestris* L. pollen tubes. Protoplasma **208:** 26–36

Feijo JA, Costa SS, Prado AM, Becker JD, Certal AC (2004) Signalling by tips. Curr Opin Plant Biol **7:** 589–598

Fernando DD (2005) Characterization of pollen tube development in *Pinus strobus* (Eastern white pine) through proteomic analysis of differentially expressed proteins. Proteomics **5:** 4917–4926

Fernando DD, Lazzaro MD, Owens JN (2005) Growth and development of conifer pollen tubes. Sex Plant Reprod **18:** 149–162

Fernando DD, Owens JN, Yu X, Ekramoddoullah AKM (2001) RNA and protein synthesis during the in vitro pollen germination and tube elongation in *Pinus monticola* and other conifers. Sex Plant Reprod **13:** 259–264

Fouquaert E, Peumans WJ, Smith DF, Proost P, Savvides SN, Van Damme EJM (2008) The "old" *Euonymus europaeus* agglutinin represents a novel family of ubiquitous plant proteins. Plant Physiol **147:** 1316–1324

Gass N, Glagotskaia T, Mellema S, Stuurman J, Barone M, Mandel T, Roessner-Tunali U, Kuhlemeier C (2005) Pyruvate decarboxylase provides growing pollen tubes with a competitive advantage in petunia. Plant Cell **17:** 2355–2368

Geitmann A, Franklin-Tong VE, Emons AC (2004) The self-incompatibility response in *Papaver rhoeas* pollen causes early and striking alterations to organelles. Cell Death Differ **11:** 812–822

Geitmann A, Snowman BN, Emons AMC, Franklin-Tong VE (2000) Alterations in the actin cytoskeleton of pollen tubes are induced by the self-incompatibility reaction in *Papaver rhoeas*. Plant Cell **12:** 1239–1251

Gibeaut DM (2000) Nucleotide sugars and glycosyltransferases for synthesis of cell wall matrix polysaccharides. Plant Physiol Biochem **38:** 69–80

Gilroy S, Hughes WA, Trewavas AJ (1987) Calmodulin antagonists increase free cytosolic calcium levels in plant protoplasts *in vivo*. FEBS Lett **212:** 133–137

Gilroy S, Trewavas AJ (2001) Signal processing and transduction in plant cells: the end of the beginning? Nat Rev Mol Cell Biol **2:** 307–314

Hao HQ, Li YQ, Hu YX, Lin JX (2005) Inhibition of RNA and protein synthesis in pollen tube development of *Pinus bungeana* by actinomycin D and cycloheximide. New Phytol **165:** 721–730

Harper JL, Daly JW (2000) Effect of calmidazolium analogs on calcium influx in HL-60 cells. Biochem Pharmacol **60:** 317–324

Hill K, Hemmler R, Kovermann P, Calenberg M, Kreimer G, Wagner R (2000) A Ca^{2+} and voltage-modulated flagellar ion channel is a component of the mechanoshock response in the unicellular green alga *Spermatozopsis similes*. Biochim Biophys Acta **1466:** 187–204

Holmes-Davis R, Tanaka CK, Vensel WH, Hurkman WJ, McCormick S (2005) Proteome mapping of mature pollen of *Arabidopsis thaliana*. Proteomics **5:** 4864–4884

Ibrahim H, Pertl H, Pittertschatscher K, Fadl-Allah E, El-Shahed A, Bentrup FW, Obermeyer G (2002) Release of an acid phosphatase activity during lily pollen tube growth involves components of the secretory pathway. Protoplasma **219:** 176–183

Imin N, Kerim T, Rolfe BG, Weinman JJ (2004) Effect of early cold stress on the maturation of rice anthers. Proteomics **4:** 1873–1882

Imin N, Kerim T, Weinman JJ, Rolfe BG (2001) Characterisation of rice anther proteins expressed at the young microspore stage. Proteomics **1:** 1149–1161

Kaplan B, Davydov O, Knight H, Galon Y, Knight MR, Fluhr R, Fromm H (2006) Rapid transcriptome changes induced by cytosolic Ca^{2+} transients reveal ABRE-related sequences as Ca^{2+}-responsive *cis* elements in *Arabidopsis*. Plant Cell **18:** 2733–2748

Kerim T, Imin N, Weinman JJ, Rolfe BG (2003) Proteome analysis of male gametophyte development in rice anthers. Proteomics **3:** 738–751

Knorpp C, Johansson M, Baird AM (2003) Plant mitochondrial nucleoside diphosphate kinase is attached to the membrane through interaction with the adenine nucleoside translocator. FEBS Lett **555:** 363–366

Korichneva I, Hammerling U (1999) F-actin as a functional target for retroretinoids: a possible role in anhydroretinol-triggered cell death. J Cell Sci **112:** 2521–2528

Krause KH, Michalak M (1997) Calreticulin. Cell **88:** 439–443

Krinke O, Novotna Z, Valentova O, Martinec J (2007) Inositol trisphosphate receptor in higher plants: is it real? J Exp Bot **58:** 361–376

Langeveld SMJ, Vennik M, Kottenhagen M, Van Wijk R, Buijk A, Kijne JW, de Pater S (2002) Glucosylation activity and complex formation of two classes of reversibly glycosylated polypeptides. Plant Physiol **100:** 278–289

Lazzaro MD, Donohue JM, Soodavar FM (2003) Disruption of cellulose synthesis by isoxaben causes tip swelling and disorganizes cortical microtubules in elongating conifer pollen tubes. Protoplasma **220:** 201–207

Ma LG, Xu XD, Cui SJ, Sun DY (1999) The presence of a heterotrimeric G protein and its role in signal transduction of extracellular calmodulin in pollen germination and tube growth. Plant Cell **11:** 1351–1363

Mascarenhas J (1993) Molecular mechanisms of pollen tube growth and differentiation. Plant Cell **5:** 1303–1314

Mellema S, Eichenberger W, Rawyler A, Suter M, Tadege M, Kuhlemeier C (2002) The ethanolic fermentation pathway supports respiration and lipid biosynthesis in tobacco pollen. Plant J **30:** 329–336

Noir S, Brautigam A, Colby T, Schmidt J, Panstruga R (2005) A reference map of the *Arabidopsis thaliana* mature pollen proteome. Biochem Biophys Res Commun **337:** 1257–1266

Parks REJ, Agarwal RP (1973) Nucleoside diphosphokinases. Enzyme **8:** 307–334

Parton RM, Parton SF, Watahiki MK, Trewavas AJ (2001) Dynamics of the

apical vesicle accumulation and the rate of growth are related in individual pollen tube. J Cell Sci 114: 2685–2695

Persson S, Wyatt SE, Love J, Thompson WF, Robertson D, Boss WF (2001) The Ca^{2+} status of the endoplasmic reticulum is altered by induction of calreticulin expression in transgenic plants. Plant Physiol 126: 1092–1104

Picton JM, Steer MW (1985) The effects of ruthenium red, lanthanum, fluorescein isothiocyanate and trifluoperazine on vesicle transport, vesicle fusion and tip extension in pollen tubes. Planta 163: 2–26

Pina C, Pinto F, Feijo JA, Becker JD (2005) Gene family analysis of the Arabidopsis pollen transcriptome reveals biological implications for cell growth, division control, and gene expression regulation. Plant Physiol 138: 744–756

Rato C, Monteiro D, Hepler PK, Malho R (2004) Calmodulin activity and cAMP signalling modulate growth and apical secretion in pollen tubes. Plant J 38: 887–897

Reddy VS, Ali GS, Reddy ASN (2002) Genes encoding calmodulin-binding proteins in the Arabidopsis genome. J Biol Chem 277: 9840–9852

Roy SJ, Holdaway-Clarke TL, Hackett GR, Kunkel JG, Lord EM, Hepler PK (1999) Uncoupling secretion and tip growth in lily pollen tubes: evidence for the role of calcium in exocytosis. Plant J 19: 379–386

Šamaj J, Müller J, Beck M, Böhm N, Menzel D (2006) Vesicular trafficking, cytoskeleton and signalling in root hairs and pollen tubes. Trends Plant Sci 11: 594–600

Šamaj J, Read ND, Volkmann D, Menzel D, Baluška F (2005) The endocytic network in plants. Trends Cell Biol 15: 425–433

Shabala SN, Newman IA, Morris J (2000) Oscillations in H$^+$ and Ca^{2+} ion fluxes around the elongation region of corn roots and effects of external pH. Plant Physiol 113: 111–118

Sheng XY, Hu ZH, Lu HF, Wang XH, Baluška F, Šamaj J, Lin JX (2006) Roles of the ubiquitin/proteasome pathway in pollen tube growth with emphasis on MG132-induced alterations in ultrastructure, cytoskeleton, and cell wall components. Plant Physiol 141: 1578–1590

Sheoran IS, Sproule KA, Olson DJH, Ross ARS, Sawhney VK (2006) Proteome profile and functional classification of proteins in *Arabidopsis thaliana* (Landsberg erecta) mature pollen. Sex Plant Reprod 19: 185–196

Shigeoka S, Ishikawa T, Tamoi M, Miyagawa Y, Takeda T, Yabuta Y, Yoshimura K (2002) Regulation and function of ascorbate peroxidase isoenzymes. J Exp Bot 53: 1305–1319

Staiger CJ, Hussey PJ (2004) Actin and actin-modulating proteins. *In* PJ Hussey, ed, The Plant Cytoskeleton in Cell Differentiation and Development. Blackwell Scientific Publications, Oxford, pp 32–80

Tadege M, Dupuis I, Kuhlemeier C (1999) Ethanolic fermentation: new functions for an old pathway. Trends Plant Sci 4: 320–325

Vandonselaar M, Hickie RA, Quail JW, Delbaere LTJ (1994) Trifluoperazine-induced conformational change in Ca^{2+}-calmodulin. Nat Struct Biol 1: 795–801

Wang QL, Lu LD, Wu XQ, Li YQ, Lin JX (2003) Boron influences pollen germination and pollen tube growth in *Picea meyeri*. Tree Physiol 23: 345–351

Williams JH (2008) Novelties of the flowering plant pollen tube underlie diversification of a key life history stage. Proc Natl Acad Sci USA 105: 11259–11263

Wu H, de Graaf B, Mariani C, Cheung AY (2001) Hydroxyproline-rich glycoproteins in plant reproductive tissues: structure, functions and regulation. Cell Mol Life Sci 58: 1418–1429

Yokota E, Muto S, Shimmen T (2000) Calcium-calmodulin suppresses the filamentous actin-binding activity of a 135-kilodalton actin-bundling protein isolated from lily pollen tubes. Plant Physiol 123: 645–654

Yoshida KT, Ohmori T, Muto S, Shimmen T (2005) cDNA microarray analysis of gene expression changes during pollination, pollen-tube elongation, fertilization, and early embryogenesis in rice pistils. Sex Plant Reprod 17: 269–275

Zhang WH, Renzel Z (1998) Determination of intracellular Ca^{2+} in cells of intact wheat root: loading of acetoxymethyl ester of Fluo-3 under low temperature. Plant J 15: 147–151